Letter

Unremovable linked nodal structures protected by crystalline symmetries in stacked bilayer graphene with Kekulé texture

Chiranjit Mondal, Sunje Kim, and Bohm-Jung Yang*
Center for Correlated Electron Systems, Institute for Basic Science (IBS), Seoul 08826, Korea;
Department of Physics and Astronomy, Seoul National University, Seoul 08826, Korea;
and Center for Theoretical Physics (CTP), Seoul National University, Seoul 08826, Korea

(Received 7 July 2022; revised 17 September 2022; accepted 20 September 2022; published 30 September 2022)

Linking structure is a new concept characterizing topological semimetals, which indicates the interweaving of gap-closing nodes at the Fermi energy (E_F) with other nodes below E_F. As the number of linked nodes can be changed only via pair creation or pair annihilation, a linked node is more stable and robust than ordinary nodes without linking. Here we propose a type of linked nodal structure between a nodal line (nodal surface) at E_F with another nodal line (nodal surface) below E_F in two-dimensional (three-dimensional) spinless fermion systems with $\mathcal{IT}$ symmetry where $\mathcal{I}$ and $\mathcal{T}$ indicate inversion and time-reversal symmetries, respectively. Because of additional chiral and rotational symmetries, in our system, a double band inversion creates a pair of linked nodes carrying the same topological charges, and thus the pair is unremovable via a Lifshiftz transition, which is clearly distinct from the cases of the linked nodes reported previously. A realistic tight-binding model and effective theory are developed for such a linking structure. Also, using density-functional-theory calculations, we propose a class of materials, composed of stacked bilayer graphene with Kekulé texture, as a candidate system hosting the linked nodal structure.

DOI: 10.1103/PhysRevB.106.L121118

Introduction. Topological semimetals and nodal superconductors indicate the gapless topological phases with nodal points (NPs)/nodal loops (NLs)/nodal surfaces (NSs) near the Fermi energy (E_F) [1–36]. Normally, such a node is characterized by its primary topological charge defined in a lowest-dimensional manifold enclosing the node such as a two-dimensional (2D) surface/one-dimensional (1D) loop/zero-dimensional (0D) point enclosing a NP/NL/NS, respectively, in a three-dimensional (3D) momentum space [24,25]. Although the presence of a primary topological charge indicates the local stability of the relevant nodal structure, it does not guarantee the global stability of the node [25,26]. For example, a single NL or NS in 3D systems with a primary topological charge can be annihilated via continuous deformation [25–27].

Recently, it was found that there is a class of doubly charged (DC) nodes with two distinct topological charges which are more robust than ordinary singly charged nodes [25–35]. Two important characteristics of DC nodes are as follows. First, the number of DC nodes can be changed only via pair creation or pair annihilation, that is, an annihilation of a single DC node is not allowed [25,26]. Second, a pair of DC nodes at E_F are linked with another node below E_F [27,28,31–34]. For example, in 3D centrosymmetric systems belonging to the Altland-Zirnbauer (AZ) [37,38] class AI and CI, a doubly charged NL at E_F is always linked with another NL below E_F [28,32].

More recently, it is found that a doubly charged NS at E_F is linked with a NL below E_F in AZ class BDI systems with inversion symmetry [34]. The full list of such linking structures and their relation with DC nodes were recently established [34] within the framework of the AZ classification, including an additional inversion $\mathcal{I}$ symmetry, dubbed the AZ+$\mathcal{I}$ classification [27]. However, understanding the influence of additional crystalline symmetries, beyond the AZ+$\mathcal{I}$ classification scheme, on the DC nodes with linking structures is still an important open problem.

In this Letter, we propose a class of linked nodal structures between two concentric NLs (NSs) at E_F and another NL (NS) below E_F in 2D (3D) spinless fermion systems belonging to the AZ+$\mathcal{I}$ class BDI with two extra symmetries: one is a threefold rotation $\mathcal{C}_{3z}$ about the z axis, and the other is a chiral symmetry $\mathcal{C}'$ that is different from the intrinsic chiral symmetry $\mathcal{C}$ of the class BDI. As both $\mathcal{C}$ and $\mathcal{C}'$ anticommute with the Hamiltonian, their combination gives a commuting symmetry $\mathcal{O}_L \equiv i\mathcal{C}\mathcal{C}'$ which is local in the momentum $\mathbf{k}$. In 2D systems, $\mathcal{O}_L$ is nothing but the mirror $\mathcal{M}_z : (x, y, z) \to (x, y, -z)$ symmetry about the basal plane of the system or a layer exchange symmetry of a 2D bilayer structure. When such 2D bilayers are vertically stacked with weak interbilayer coupling, $\mathcal{O}_L$ still remains as an excellent $\mathbf{k}$-local symmetry of the resulting 3D structure, which supports linked NSs. Interestingly, in this class of systems, a double band inversion (DBI) creates two concentric NLs or NSs at E_F that carry two distinct 0D topological charges: one is Z_2 type (Z_2^{0D}) while the other is Z type (Z^{0D}). As the two NLs (NSs) at E_F have the same Z-type charges, their pair annihilation through a Lifshitz transition is forbidden. Such a stability against the

*bjyang@snu.ac.kr

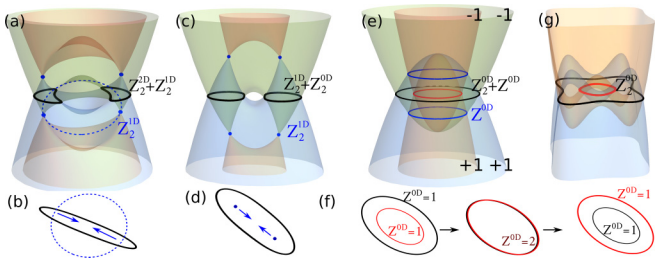

FIG. 1. (a) Linked nodes in 3D systems belonging to the AZ+$\mathcal{I}$ class AI or CI. A monopole NL at E_F (black loop) is linked with another NL below E_F (blue dotted loop). Z^{dD} (Z_2^{dD}) ($d = 0, 1, 2$) near each node indicates its d-dimensional Z (Z_2) charge. The relevant nodal structure after merging of two monopole NLs is shown in (b). Both the merged NL at E_F and the NL below E_F can be annihilated. (c) Linked nodes in 2D systems belonging to the AZ+$\mathcal{I}$ class BDI. A NL at E_F (black loop) always accompanies a NP below E_F (blue dot). The relevant nodal structure after merging of two NLs is shown in (d). Both the merged NL at E_F and two NPs below E_F can be annihilated. (e) Linked nodes in 2D systems belonging to the AZ+$\mathcal{I}$ class BDI with additional chiral and $\mathcal{C}_{3z}$ symmetries. ± 1 denotes $\mathcal{O}_L$ eigenvalues. Two concentric NLs at E_F accompany another NL below E_F. The merging process of two concentric NLs at E_F is described in (f). As they have the same Z^{0D}, pair annihilation is impossible. (g) Two concentric NLs generated by a single band inversion. Two loops can be pair annihilated.

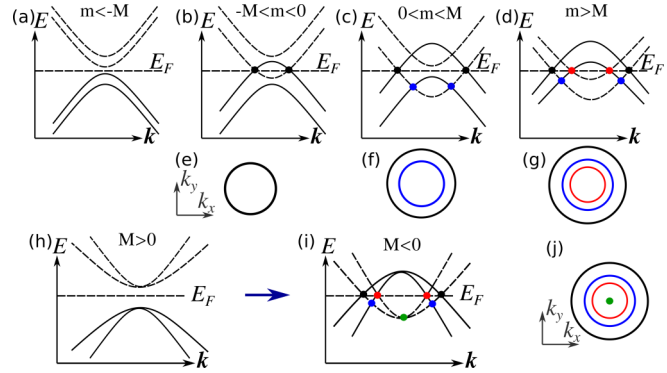

FIG. 2. (a, b, c, d) A double band inversion (DBI) process in systems belonging to the AZ+$\mathcal{I}$ class BDI with an additional chiral symmetry $\mathcal{C}'$. (e, f, g) The nodal structure corresponding to each upper panel. (h, i) BDI process when extra $\mathcal{C}_{3z}$ symmetry is included. (j) The nodal structure corresponding to (i). The solid (dashed) lines indicate the bands carrying $+1$ (-1) $\mathcal{O}_L$ eigenvalues.

pair annihilation does not exist in any other DC nodes known up to now.

We construct a realistic model and symmetry-based effective theory considering a Kekulé textured bilayer graphene (BLG) and the related layered 3D structure as an example. Also, using the *ab initio* band structure calculations, we propose a class of materials with the chemical formula AC_{12} (A = Zn, Al, Be) in which the interplay of two distinct chiral symmetries and $\mathcal{C}_{3z}$ protects the linked cylindrical NSs near E_F. We also show that breaking the chiral symmetries transforms the NSs to NLs as realized in materials BC_{12} (B = Li, B, Mg) in which NLs are protected by $\mathcal{IT}$ and $\mathcal{M}_z$ symmetry, where $\mathcal{T}$ indicates time-reversal ($\mathcal{T}$) symmetry.

Double band inversion (DBI) and linking structure. A pair of DC nodes with linking structure can be created via a DBI process in which two valence and two conduction bands are simultaneously inverted. For instance, in a 3D system belonging to the AZ+$\mathcal{I}$ class AI or CI, a DBI creates a pair of monopole NLs at E_F that carry both a 1D Z_2 charge Z_2^{1D} (equivalent to the π Berry phase) and a 2D Z_2 monopole charge Z_2^{2D} as described in Fig. 1(a) [28]. Each monopole NL at E_F (black loop) is always linked with another NL below E_F (blue dashed loop) [28]. When the band structure is smoothly deformed in a way that two monopole NLs merge and turn into a single trivial NL without monopole charge, both the trivial NL at E_F and the NL below E_F can be continuously shrunk to a point and then be annihilated [see Fig. 1(b)]. A similar deformation is also possible in 2D systems belonging to the AZ+$\mathcal{I}$ class BDI, where a NL at E_F is linked with a NP below E_F [34] [see Fig. 1(c)]. When two DC NLs at E_F are merged, both the merged NL at E_F and the NP pair below E_F can be annihilated as described in Fig. 1(d).

On the other hand, when an additional chiral symmetry and $\mathcal{C}_{3z}$ are supplemented to the 2D class BDI systems, a distinct type of DC NLs with extra stability can be created via a DBI. In this case, each of the NLs at E_F carries two distinct 0D charges (Z_2^{0D} and Z^{0D}), and the two NLs at E_F are linked with another NL below E_F as shown in Fig. 1(e). Interestingly, when the two concentric NLs at E_F are merged, as they have the same Z^{0D} charge, the merged NL also carries a nonzero topological charge so that it cannot be annihilated. Thus further deformation splits the merged NL into two DC concentric NLs again as described in Fig. 1(f). We note that the emergence of concentric DC NLs is a direct consequence of a DBI. In contrast, when two concentric NLs are created by a single band inversion between one valence and one conduction band as in Fig. 1(g), the merging of two concentric NLs always leads to their pair annihilation and gap opening.

Continuum Hamiltonian. A general DBI process of 2D systems belonging to the AZ+$\mathcal{I}$ class BDI can be described by the following four-band continuum Hamiltonian:

$$H(\mathbf{k}) = p(\mathbf{k})\sigma_z\tau_0 + q(\mathbf{k})\sigma_z\tau_x + r(\mathbf{k})\sigma_z\tau_z + s(\mathbf{k})\sigma_y\tau_y, \quad (1)$$

where the functions $p(\mathbf{k})$, $q(\mathbf{k})$, $r(\mathbf{k})$, and $s(\mathbf{k})$ are even in the momentum $\mathbf{k}$. Using the Pauli matrices $\tau_{x,y,z}$, $\sigma_{x,y,z}$, 2×2 identity matrices σ_0, τ_0, and the complex conjugation operator K, we choose the symmetry representation $\mathcal{I} = \sigma_0\tau_0$, $\mathcal{T} = K\sigma_0\tau_0$, and $\mathcal{C} = \sigma_x\tau_0$, which satisfies $(\mathcal{IT})^2 = \mathcal{C}^2 = 1$. Also, the combination of $\mathcal{IT}$ and $\mathcal{C}$ gives a $\mathbf{k}$-local particle-hole symmetry $\mathcal{P} = \mathcal{ITC}$. Then the Hamiltonian satisfies $(\mathcal{IT})H(\mathbf{k})(\mathcal{IT})^{-1} = H(\mathbf{k})$, $\mathcal{P}H(\mathbf{k})\mathcal{P}^{-1} = -H(\mathbf{k})$, and $\mathcal{C}H(\mathbf{k})\mathcal{C}^{-1} = -H(\mathbf{k})$, which are the defining property of the AZ+$\mathcal{I}$ class BDI. We also impose $\mathcal{I}$ symmetry as the DBI occurs at the Γ point. When an additional chiral symmetry $\mathcal{C}' = \sigma_y\tau_0$ exists, we find $s(\mathbf{k}) = 0$ and $[H(\mathbf{k}), \mathcal{O}_L] = 0$, where $\mathcal{O}_L = i\mathcal{CC}'$.

To describe a DBI process, we assume $p(\mathbf{k}) = M$, $q(\mathbf{k}) = k^2 - m$, $r(\mathbf{k}) = s(\mathbf{k}) = 0$ where $M > 0$ and m are constants. As shown in Fig. 2, when $m < -M$, we have a gapped band structure. When $-M < m < 0$, a NL appears at E_F. When $0 < m < M$, another NL emerges below E_F. Finally, when

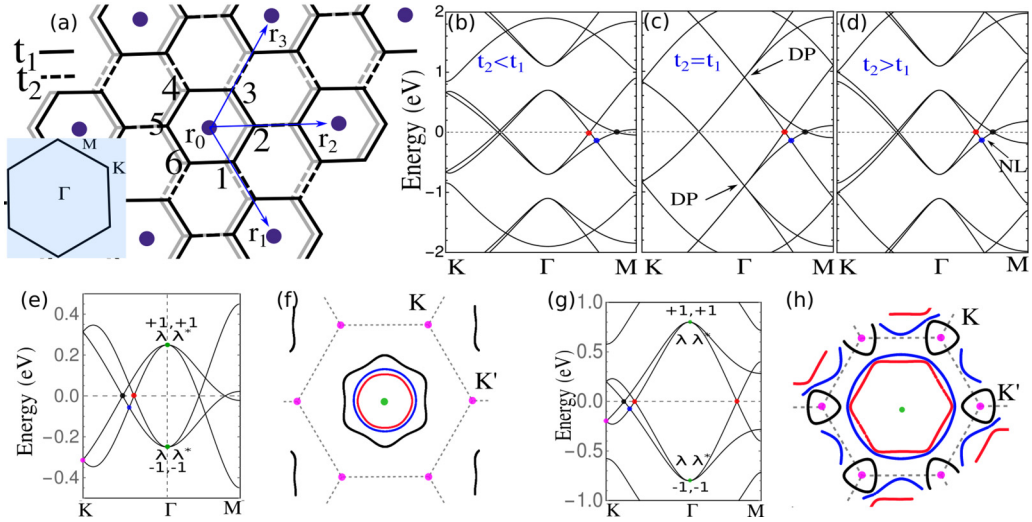

FIG. 3. (a) Structure of Kekulé textured AA-stacked bilayer graphene (KABLG). t_1 (t_2) indicates the intracell (intercell) hopping represented by solid (dashed) bonds. The relevant first Brillouin zone (BZ) is shown in the inset. (b, c, d) The band structures of KABLG when (b) $t_2 < t_1$ (anti-Kekulé texture), (c) $t_2 = t_1$, and (g) $t_2 > t_1$ (Kekulé texture). In all cases, the same interlayer coupling $|t_3| < |t_1|, |t_2|$ is used. (e, f) The band and nodal structures of KABLG near E_F for parameters $t_1 = 1, t_2 = 0.6$, and $t_3 = 0.8$. ± 1 (λ, λ^*) denote the $\mathcal{O}_L$ ($\mathcal{C}_{3z}$) eigenvalues. (g, h) The band and nodal structures near E_F when $t_3 = 1.2$ after a Lifshitz transition of the black NL through the BZ boundary. In (e, f, g, h), the red and black NLs are at E_F while the blue NL is below E_F. The magenta (green) NPs are below E_F at the momentum $\mathbf{K}/\mathbf{K}'$ (Γ).

$m > M$, the second NL at E_F is generated, and thus we have two concentric NLs at E_F linked with another NL below E_F. We see that although a linked nodal structure can be created via a sequence of BDI process described in Figs. 2(a)–2(d), the NLs at E_F are created individually, not pairwise. However, when $\mathcal{C}_{3z}$ symmetry that imposes double degeneracy at $\mathbf{k} = 0$ is supplemented, the DBI process for the pair creation of concentric NLs can be completed as shown in Figs. 2(h)–2(j).

To implement $\mathcal{C}_{3z}$ symmetry, we take a matrix representation $\mathcal{C}_{3z} = e^{i\frac{2\pi}{3}\sigma_0\tau_y}$ satisfying $(C_{3z})^3 = 1$, $[C_{3z}, \mathcal{T}] = 0$. The $\mathcal{C}_{3z}$ invariance of the Hamiltonian can be satisfied by choosing $p(\mathbf{k}) = M + 2\alpha(k_x^2 + k_y^2)$, $q(\mathbf{k}) = -2\alpha k_x k_y$, $r(\mathbf{k}) = \alpha(k_x^2 - k_y^2)$. Assuming $\alpha > 0$, we have a gapped band structure when $M > 0$, as shown in Fig. 2(h), in which double degeneracy occurs at Γ because the bands have complex $\mathcal{C}_{3z}$ eigenvalues $\lambda = e^{i2\pi/3}$ and λ^*. One can also show that the $\mathcal{O}_L$ eigenvalues of the unoccupied (occupied) bands are $+1$ (-1) after DBI, and all four bands have the same inversion eigenvalues at Γ. When $M < 0$, two NLs appear at E_F with radii $\sqrt{|M|/\alpha}$ and $\sqrt{|M|/3\alpha}$, respectively. Between them, another NL with a radius $\sqrt{|M|/2\alpha}$ appears below E_F.

Topological charges. Let us define Z^{0D} and Z_2^{0D}, explicitly. First, Z^{0D} is defined by the eigenvalues (± 1) of $\mathcal{O}_L$ symmetry. At a given momentum $\mathbf{k}$, we denote the number of occupied bands with the positive (negative) $\mathcal{O}_L$ eigenvalues by $\eta_+(\mathbf{k})$ ($\eta_-(\mathbf{k})$. Also, we define $\Delta\eta(\mathbf{k}) = \eta_+(\mathbf{k}) - \eta_-(\mathbf{k})$. For a given NL, we pick two momenta $\mathbf{k}_{\rm in}$ and $\mathbf{k}_{\rm out}$, which are inside and outside of the loop, respectively. Then we define $Z^{0D} \equiv \frac{1}{2}[\Delta\eta(\mathbf{k}_{\rm out}) - \Delta\eta(\mathbf{k}_{\rm in})]$. One can easily show that $Z^{0D} = +1$ for both NLs at E_F in Figs. 2(d) and 2(i).

Another charge Z_2^{0D} is defined as follows [27]. Due to chiral symmetry, $H(\mathbf{k})$ can take a block off-diagonal form as $H(\mathbf{k}) = \begin{pmatrix} 0 & A(\mathbf{k}) \\ A^T(\mathbf{k}) & 0 \end{pmatrix}$, where $A(\mathbf{k})$ denotes a real matrix. Then Z_2^{0D} is defined as

$$Z_2^{0D} = \text{sign}\{\det A(\mathbf{k}_{\rm in}) \cdot \det A(\mathbf{k}_{\rm out})\}. \tag{2}$$

It is straightforward to show that the two concentric NLs at E_F in Figs. 2(d) and 2(i) have opposite Z_2^{0D} charges.

Kekulé-textured AA-stacked bilayer graphene (KABLG). The proposed 2D linked nodal structure can be realized in AA-stacked bilayer graphene (BLG) with Kekulé-O distortion [40,41], which indicates the bond modulation pattern shown in Fig. 3(a) in which the intracell hopping t_1 within a hexagonal unit cell is distinguished from the intercell hopping t_2. When two graphene layers with Kekulé-O distortion are vertically stacked (AA stacking), we obtain the KABLG, which can be realized by inserting metal ions between graphene layers.

We consider the following 12×12 tight-binding Hamiltonian for KABLG, $H_{KABLG} = \sigma_0 \otimes H_{KSLG} + \sigma_x \otimes H_c$, where the Pauli matrices $\sigma_{x,y,z}$ denote the layer degrees of freedom and σ_0 is the related identity matrix. H_{KSLG} indicates the Hamiltonian for a Kekulé-textured single layer graphene (KSLG) given by $H_{KSLG} = -\sum_{<i,j>} t_{ij} c_i^\dagger c_j + \text{H.c.}$, where c_i denotes the electron annihilation operator at the ith site, and $t_{ij} = t_1$ ($t_{ij} = t_2$) for the intracell (intercell) hopping between nearest-neighboring sites. $H_c = diag[t_3, t_3, t_3, t_3, t_3, t_3]$ describes the interlayer hopping with the amplitude t_3 for nearest neighboring atoms between layers. H_{KABLG} has $\mathcal{I}$, $\mathcal{T}$, $\mathcal{C}$, $\mathcal{C}'$ symmetries represented by $\mathcal{I} = \sigma_x \otimes \tau_x \otimes I_3$, $\mathcal{T} = K\sigma_0 \otimes \tau_0 \otimes I_3$, $\mathcal{C} = \sigma_z \otimes \tau_z \otimes I_3$, $\mathcal{C}' = \sigma_y \otimes \tau_z \otimes I_3$, where I_3 is a 3×3 identity matrix related to the trimerization of the graphene unit cell induced by Kekulé-O distortion. The Pauli matrices $\tau_{x,y,z}$ denote the sublattice degrees of freedom, and τ_0 is the related identity matrix.

Depending on the type of metal ions, the textured lattice can be in a phase with $t_2 < t_1$ (anti-Kekulé distortion) or $t_2 >$

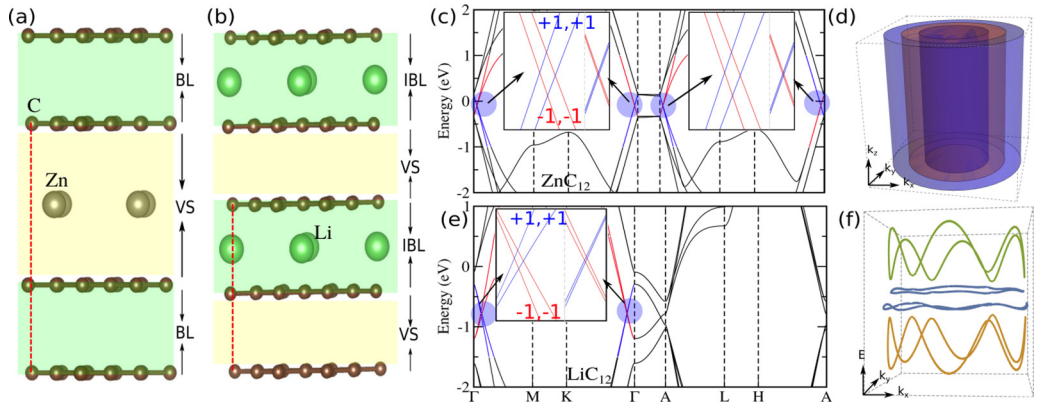

FIG. 4. (a) Schematic structure of ZnC_{12}, a stacked BLG system with Zn atoms between neighboring BLGs. Weak (repulsive) interaction between Zn atoms and BLG induces Kekulé-O type distortion of BLGs. Here BL (VS) indicates the bilayer (vdW spacing). (b) Schematic structure of LiC_{12} where strong interaction between Li^+ ions and neighboring graphene layers gives intercalated bilayers (IBLs). The red dashed vertical lines in (a, b) represent the unit cell length along the z direction. (c, e) Bulk band structures of (c) ZnC_{12} and (e) LiC_{12}. Blue shaded regions represent the nodal degeneracies with close-up views in the inset. ± 1 represents $\mathcal{O}_L$ ($\mathcal{M}_z$) eigenvalues in (c) [(e)]. (d) Schematic plot of the cylindrical concentric NSs at E_F (blue) of ZnC_{12} linked with another NS below E_F (red). (f) NLs of LiC_{12} on the $k_z = 0$ plane protected by $\mathcal{IT}$ and $\mathcal{M}_z$ symmetries.

t_1 (Kekulé distortion), as shown in Figs. 3(b)–3(d). In both cases, the nonzero interlayer hopping (t_3) pushes the gapped band structure of each textured graphene layer upward and downward in energy, respectively, which generates linked NLs similar to those in Fig. 1(e).

The low-energy band structures are similar in both $t_2 < t_1$ and $t_1 < t_2$ cases. For convenience, here we focus on the $t_2 < t_1$ case. The $t_2 > t_1$ case is discussed in the Supplemental Material (SM) [39]. As shown in Figs. 3(e) and 3(f), the band and nodal structures of the four bands near E_F are identical to those in Figs. 2(i) and 2(j) with linked NLs. As the two NLs at E_F carry the same Z^{0D} charge, they cannot be pair annihilated through merging.

As shown in Figs. 3(g) and 3(h), as t_3 increases, the size of the outer NL at E_F becomes larger, and after touching the BZ boundary, it splits into two NLs encircling K and K', respectively. Interestingly, each of this NL develops another type of the linked nodal structure with a NP below E_F [34]. As each NL at K or K' is DC, it cannot be annihilated separately (see SM [39]). This is another way that the stability of two concentric NLs is manifested.

Candidate materials. We propose a class of 3D materials with chemical formula MC_{12} (M: a metal ion) as a candidate system that exhibits the linked nodal structure discussed above. We note that although the discussion up to now has been focused on 2D bilayer systems, the same idea can be applied to 3D systems obtained by vertical stacking of 2D bilayers. The linked concentric NLs in 2D bilayer systems can be naturally extended to the linked concentric NSs, as long as the coupling between neighboring bilayers is weak enough so that the system preserves the same symmetries including $\mathcal{C}$ and $\mathcal{C}'$.

MC_{12} has a hexagonal crystal structure with space group $P6/mmm$, composed of van der Waals (vdW) stacking of BLGs with intercalated M ions. Specifically, in ZnC_{12} shown in Fig. 4(a), the chemical interaction between Zn and C atoms is relatively weak, which can be supported by the fact that the optimized bond distance between Zn and C atoms is 3.40 Å, which is larger than the sum of their vdW interaction lengths 3.10 Å. Although chiral symmetry is not exact in any material, it is an excellent symmetry in ZnC_{12} due to the weak interaction between BLG layers. Accordingly, ZnC_{12} can support linked cylindrical NSs.

The electronic structures of ZnC_{12} are shown in Fig. 4(c). In ZnC_{12} with $\mathcal{O}_L$ symmetry, a DBI appears between two pairs of bands with different $\mathcal{O}_L$ eigenvalues along Γ-A direction. The DBI generates two NSs near E_F and another NS below the E_F between them, as schematically described in Fig. 4(d). Similar linked NSs can appear in various materials, including AlC_{12}, BeC_{12} in which a DBI occurs along the entire Γ-A direction (see SM [39]).

On the other hand, the situation changes dramatically in a related compound LiC_{12} [see Fig. 4(b)]. In LiC_{12}, the optimized distance between Li and C atoms is 2.35 Å, which is much smaller than the sum of their vdW interaction lengths 3.52 Å. This is because of the ionic nature of Li atoms which strongly interact with the carbon p_z orbitals in graphene. Thus, in contrast to ZnC_{12}, LiC_{12} allows the second-nearest-neighbor hopping between the layers mediated by Li ions, which breaks both chiral symmetries. Thus, the NSs, which exist when chiral symmetries present, are mostly gapped except in the $k_z = 0$ plane. However, as the $\mathcal{IT}$ symmetry still exists, the compound can have NLs [28] with drumhead surface states on the boundary. The NLs in LiC_{12} are shown in Fig. 4(f), and the related surface states are described in the SM [39].

Discussions. Finally, let us discuss the experimental feasibility of our proposed model and related materials. Various Kekulé-O ordered BLG systems have been synthesized and studied using angle-resolved photoemission spectroscopy (ARPES) and transport measurements [40,42–46]. For instance, the gap opening at the Dirac cone due to chiral symmetry breaking was observed in LiC_{12} from ARPES measurement [40]. Similarly, CaC_{12} was also synthesized experimentally to study superconductivity [44,45]. Moreover, the chemical stability of ZnC_{12} was theoretically shown by

Srimanta *et al.* [47] in which the binding energies of various transition metal intercalated BLG were computed [47]. Various other types of atoms such as Yb [48], Eu [48], and Ge [49] have been intercalated in similar BLG structures, and their electronic structures have been explored using ARPES. All these works strongly support the possible experimental realization of our predicted linked nodal structures in future experiments. As the topological charges of nodes are closely tied in with the linking structure between nodes, the measurement of the global band structure of linked nodes would provide a direct experimental evidence of nontrivial topological charges of the linked semimetals proposed in this work.

Acknowledgments. C.M. thanks R. Ghadimi for fruitful discussions. C.M., S.K., and B.J.Y. were supported by the Institute for Basic Science in Korea (Grant No. IBS-R009-D1), Samsung Science and Technology Foundation under Project No. SSTF-BA2002-06, and a National Research Foundation of Korea (NRF) grant funded by the Korea Government (MSIT) (No. 2021R1A2C4002773 and No. NRF-2021R1A5A1032996).

[1] N. P. Armitage, E. J. Mele, and A. Vishwanath, Weyl and Dirac semimetals in three-dimensional solids, Rev. Mod. Phys. **90**, 015001 (2018).

[2] H. Weng, C. Fang, Z. Fang, B. A. Bernevig, and X. Dai, Weyl Semimetal Phase in Noncentrosymmetric Transition-Metal Monophosphides, Phys. Rev. X **5**, 011029 (2015).

[3] S.-Y. Xu, I. Belopolski, N. Alidoust, M. Neupane, G. Bian, C. Zhang, R. Sankar, G. Chang, Z. Yuan, C.-C. Lee *et al.*, Discovery of a Weyl fermion semimetal and topological Fermi arcs, Science **349**, 613 (2015).

[4] C. Fang, M. J. Gilbert, X. Dai, and B. A. Bernevig, Multi-Weyl Topological Semimetals Stabilized by Point Group Symmetry, Phys. Rev. Lett. **108**, 266802 (2012).

[5] B.-J. Yang and N. Nagaosa, Classification of stable three-dimensional Dirac semimetals with nontrivial topology, Nat. Commun. **5**, 4898 (2014).

[6] Z. K. Liu, B. Zhou, Y. Zhang, Z. J. Wang, H. M. Weng, D. Prabhakaran, S.-K. Mo, Z. X. Shen, Z. Fang, X. Dai, Z. Hussain, and Y. L. Chen, Discovery of a Three-Dimensional Topological Dirac Semimetal, Na_3Bi, Science **343**, 864 (2014).

[7] S. M. Young, S. Zaheer, J. C. Y. Teo, C. L. Kane, E. J. Mele, and A. M. Rappe, Dirac Semimetal in Three Dimensions, Phys. Rev. Lett. **108**, 140405 (2012).

[8] M. Neupane, S.-Y. Xu, R. Sankar, N. Alidoust, G. Bian, C. Liu, I. Belopolski, T.-R. Chang, H.-T. Jeng, H. Lin, A. Bansil, F. Chou, and M. Z. Hasan, Observation of a three-dimensional topological Dirac semimetal phase in high-mobility Cd_3As_2, Nat. Commun. **5**, 3786 (2014).

[9] Y. Kim, B. J. Wieder, C. L. Kane, and A. M. Rappe, Dirac Line Nodes in Inversion-Symmetric Crystals, Phys. Rev. Lett. **115**, 036806 (2015).

[10] R. Yu, H. Weng, Z. Fang, X. Dai, and X. Hu, Topological Node-Line Semimetal and Dirac Semimetal State in Antiperovskite Cu_3PdN, Phys. Rev. Lett. **115**, 036807 (2015).

[11] L. M. Schoop, M. N. Ali, C. Straber, A. Topp, A. Varykhalov, D. Marchenko, V. Duppel, S. S. P. Parkin, B. V. Lotsch, and C. R. Ast, Dirac cone protected by non-symmorphic symmetry and three-dimensional Dirac line node in ZrSiS, Nat. Commun. **7**, 11696 (2016).

[12] Z. Liu, R. Lou, P. Guo, Q. Wang, S. Sun, C. Li, S. Thirupathaiah, A. Fedorov, D. Shen, K. Liu, H. Lei, and S. Wang, Experimental Observation of Dirac Nodal Links in Centrosymmetric Semimetal TiB_2, Phys. Rev. X **8**, 031044 (2018).

[13] X. Zhang, Z.-M. Yu, X.-L. Sheng, H. Y. Yang, and S. A. Yang, Coexistence of four-band nodal rings and triply degenerate nodal points in centrosymmetric metal diborides, Phys. Rev. B **95**, 235116 (2017).

[14] A. Yamakage, Y. Yamakawa, Y. Tanaka, and Y. Okamoto, Line-Node Dirac Semimetal and Topological Insulating Phase in Noncentrosymmetric Pnictides CaAgX (X = P, As), J. Phys. Soc. Jpn. **85**, 013708 (2016).

[15] I. Belopolski, G. Chang, T. A. Cochran, Z.-J. Cheng, X. P. Yang, C. Hugelmeyer, K. Manna, J.-X. Yin, G. Cheng, D. Multer *et al.*, Observation of a linked-loop quantum state in a topological magnet, Nature (London) **604**, 647 (2022).

[16] J. D. Sau and S. Tewari, Topologically protected surface Majorana arcs and bulk Weyl fermions in ferromagnetic superconductors, Phys. Rev. B **86**, 104509 (2012).

[17] T. Meng and L. Balents, Weyl superconductors, Phys. Rev. B **86**, 054504 (2012).

[18] Y. X. Zhao, A. P. Schnyder, and Z. D. Wang, Unified Theory of PT and CP Invariant Topological Metals and Nodal Superconductors, Phys. Rev. Lett. **116**, 156402 (2016).

[19] M. H. Fischer, M. Sigrist, and D. F. Agterberg, Superconductivity without Inversion and Time-Reversal Symmetries, Phys. Rev. Lett. **121**, 157003 (2018).

[20] S. Sumita, T. Nomoto, K. Shiozaki, and Y. Yanase, Classification of topological crystalline superconducting nodes on high-symmetry lines: Point nodes, line nodes, and Bogoliubov Fermi surfaces, Phys. Rev. B **99**, 134513 (2019).

[21] S. Kobayashi, S. Sumita, Y. Yanase, and M. Sato, Symmetry-protected line nodes and Majorana flat bands in nodal crystalline superconductors, Phys. Rev. B **97**, 180504(R) (2018).

[22] J. Ahn, S. Park, and B.-J. Yang, Failure of Nielsen-Ninomiya Theorem and Fragile Topology in Two-Dimensional Systems with Space-Time Inversion Symmetry: Application to Twisted Bilayer Graphene at Magic Angle, Phys. Rev. X **9**, 021013 (2019).

[23] A. Bouhon, Q. Wu, R.-J. Slager, H. Weng, O. V. Yazyev, and T. Bzdušek, Non-Abelian reciprocal braiding of Weyl points and its manifestation in ZrTe, Nat. Phys. **16**, 1137 (2020).

[24] O. Vafek and A. Vishwanath, Dirac Fermions in Solids: From High-Tc Cuprates and Graphene to Topological Insulators and Weyl Semimetals, Annu. Rev. Condens. Matter Phys. **5**, 83 (2014).

[25] C. Fang, H. Weng, X. Dai, and Z. Fang, Topological nodal line semimetals, Chin. Phys. B **25**, 117106 (2016).

[26] C. Fang, Y. Chen, H.-Y. Kee, and L. Fu, Topological nodal line semimetals with and without spin-orbital coupling, Phys. Rev. B **92**, 081201(R) (2015).

[27] T. Bzdušek and M. Sigrist, Robust doubly charged nodal lines and nodal surfaces in centrosymmetric systems, Phys. Rev. B **96**, 155105 (2017).

[28] J. Ahn, D. Kim, Y. Kim, and B.-J. Yang, Band Topology and Linking Structure of Nodal Line Semimetals with Z_2 Monopole Charges, Phys. Rev. Lett. **121**, 106403 (2018).

[29] H. Li, C. Fang, and K. Sun, Diagnosis of topological nodal lines with nontrivial monopole charge in the presence of rotation symmetries, Phys. Rev. B **100**, 195308 (2019).

[30] Z. Song, T. Zhang, and C. Fang, Diagnosis for Nonmagnetic Topological Semimetals in the Absence of Spin-Orbital Coupling, Phys. Rev. X **8**, 031069 (2018).

[31] Q. S. Wu, A. A. Soluyanov, and T. Bzdušek, Non-Abelian band topology in noninteracting metals, Science **365**, 1273 (2019).

[32] A. Tiwari and T. Bzdušek, Non-Abelian topology of nodal-line rings in PT-symmetric systems, Phys. Rev. B **101**, 195130 (2020).

[33] A. Bouhon and R.-J. Slager, Multi-gap topological conversion of Euler class via band-node braiding: Minimal models, PT-linked nodal rings, and chiral heirs, arXiv:2203.16741.

[34] S. Kim, D.-C. Ryu, and B.-J. Yang, Linking structures of doubly charged nodal surfaces in centrosymmetric superconductors, Phys. Rev. B **103**, 224523 (2021).

[35] Z. Wang, B. J. Wieder, J. Li, B. Yan, and B. A. Bernevig, Higher-Order Topology, Monopole Nodal Lines, and the Origin of Large Fermi Arcs in Transition Metal Dichalcogenides XTe_2 (X=Mo, W), Phys. Rev. Lett. **123**, 186401 (2019).

[36] C. Chen, X-T. Zeng, Z. Chen, Y. X. Zhao, X-L. Sheng, and A. Y. Shengyuan, Second-Order Real Nodal-Line Semimetal in Three-Dimensional Graphdiyne, Phys. Rev. Lett. **128**, 026405 (2022).

[37] A. Altland and M. R. Zirnbauer, Nonstandard symmetry classes in mesoscopic normal-superconducting hybrid structures, Phys. Rev. B **55**, 1142 (1997).

[38] S. Ryu, A. P. Schnyder, A. Furusaki, and Andreas W. W. Ludwig, Topological insulators and superconductors: Tenfold way and dimensional hierarchy, New J. Phys. **12**, 065010 (2010).

[39] See Supplemental Material at http://link.aps.org/supplemental/10.1103/PhysRevB.106.L121118 for details of the tight binding lattice model, linking structure of BDI class, methodology of DFT calculations, and band structures of additional materials, which includes Refs. [50–60].

[40] C. Bao, H. Zhang, T. Zhang, X. Wu, L. Luo, S. Zhou, Q. Li, Y. Hou, W. Yao, L. Liu, P. Yu, J. Li, W. Duan, H. Yao, Y. Wang, and S. Zhou, Experimental Evidence of Chiral Symmetry Breaking in Kekulé-Ordered Graphene, Phys. Rev. Lett. **126**, 206804 (2021).

[41] C. Bao, H. Zhang, X. Wu, S. Zhou, Q. Li, P. Yu, J. Li, W. Duan, and S. Zhou, Coexistence of extended flat band and Kekulé order in Li-intercalated graphene, Phys. Rev. B **105**, L161106 (2022).

[42] K. Sugawara, K. Kanetani, T. Sato, and T. Takahashi, Fabrication of Li-intercalated bilayer graphene, AIP Adv. **1**, 022103 (2011).

[43] S. Fiori, Y. Murata, S. Veronesi, A. Rossi, C. Coletti, and S. Heun, Li-intercalated graphene on SiC(0001): An STM study, Phys. Rev. B **96**, 125429 (2017).

[44] S. Ichinokura, K. Sugawara, A. Takayama, T. Takahashi, and S. Hasegawa, Superconducting Calcium-Intercalated Bilayer Graphene, ACS Nano **10**, 2761 (2016).

[45] K. Kanetani, K. Sugawara, T. Sato, R. Shimizu, K. Iwaya, T. Hitosugi, and T. Takahashi, Ca intercalated bilayer graphene as a thinnest limit of superconducting C_6Ca, Proc. Natl. Acad. Sci. USA **109**, 19610 (2012).

[46] C. Gutiérrez, C.-J. Kim, L. Brown, T. Schiros, D. Nordlund, E. B. Lochocki, K. M. Shen, J. Park, and A. N. Pasupathy, Imaging chiral symmetry breaking from Kekulé bond order in graphene, Nat. Phys. **12**, 950 (2016).

[47] S. Pakhira and J. L. Mendoza-Cort, Tuning the Dirac cone of bilayer and bulk structure graphene by intercalating first row transition metals using first-principles calculations, J. Phys. Chem. C **122**, 4768 (2018).

[48] S. L. Molodtsov, C. Laubschat, M. Richter, T. Gantz, and A. M. Shikin, Electronic structure of Eu and Yb graphite intercalation compounds, Phys. Rev. B **53**, 16621 (1996).

[49] K. V. Emtsev, A. A. Zakharov, C. Coletti, S. Forti, and U. Starke, Ambipolar doping in quasifree epitaxial graphene on SiC(0001) controlled by Ge intercalation, Phys. Rev. B **84**, 125423 (2011).

[50] P. E. Blöchl, Projector augmented-wave method, Phys. Rev. B **50**, 17953 (1994).

[51] G. Kresse and J. Hafner, *Ab initio* molecular dynamics for liquid metals, Phys. Rev. B **47**, 558(R) (1993).

[52] G. Kresse and D. Joubert, From ultrasoft pseudopotentials to the projector augmented-wave method, Phys. Rev. B **59**, 1758 (1999).

[53] N. Marzari and D. Vanderbilt, Maximally localized generalized Wannier functions for composite energy bands, Phys. Rev. B **56**, 12847 (1997).

[54] I. Souza, N. Marzari, and D. Vanderbilt, Maximally localized Wannier functions for entangled energy bands, Phys. Rev. B **65**, 035109 (2001).

[55] N. Marzari, A. A. Mostofi, J. R. Yates, I. Souza, and D. Vanderbilt, Maximally localized Wannier functions: Theory and applications, Rev. Mod. Phys. **84**, 1419 (2012).

[56] A. A. Mostofi, J. R. Yates, G. Pizzi, Y. S. Lee, I. Souza, D. Vanderbilt, and N. Marzari, wannier90: A tool for obtaining maximally-localised Wannier functions, Comput. Phys. Commun. **185**, 2309 (2014)

[57] D. H. Lee and J. D. Joannopoulos, Simple scheme for surface-band calculations. I. Phys. Rev. B **23**, 4988 (1981).

[58] D. H. Lee and J. D. Joannopoulos, Simple scheme for surface-band calculations. II. The Green's function, Phys. Rev. B **23**, 4997 (1981).

[59] M. P. Lopez Sancho, J. M. Lopez Sancho, J. M. L. Sancho, and J. Rubio, Highly convergent schemes for the calculation of bulk and surface Green functions, J. Phys. F: Met. Phys. **15**, 851 (1985).

[60] Q.-S. Wu, S.-N. Zhang, H.-F. Song, M. Troyer, and A. A. Soluyanov, WannierTools: An open-source software package for novel topological materials, Comput. Phys. Commun. **224**, 405 (2018).